PERGAMON

International Journal of Solids and Structures 37 (2000) 515–533

INTERNATIONAL JOURNAL OF SOLIDS and STRUCTURES

www.elsevier.com/locate/ijsolstr

The hockling of cables: a problem in shearable and extensible rods

D.M. Stump*

Department of Mathematics, The University of Queensland, St. Lucia, Qld 4072, Australia

Received 17 August 1998; in revised form 11 December 1998

Abstract

In certain industrial processes, such as undersea cable laying, a very long rod subject to remote axial tension and torque can form a self-contacting loop. An increase in remote tension under a fixed torque can draw the loop down in size until it becomes very small and then pulls apart. The very large local strains of the small loop can permanently damage the rod (e.g. through plastic deformation). In the cable laying industry, this process is known as *hockling*.

This study uses the theory of linear elastic rods which can undergo shear and extensional deformations in addition to bending and twisting curvatures in order to solve approximately for the shape, force, and moments that occur during hockling. A new closed-form solution to the rod theory equations is developed and used to predict (at least approximately) the loops sizes and remote tensions that occur at the formation and pull apart of the contacting loop.

Keywords: Shearable and extensible rods; Homoclinic solutions; Nonlinear kinematics; Cable hockling; Coyne solution

1. Introduction

A variety of industrial processes over a range of length scales involve the manipulation of elastic rod structures that are subject to remote applied tension and twist (e.g. textile yarn production and under sea cable laying). During the handling of these rods a loop can 'pop' into the shape for a variety of reasons such as material or loading nonuniformities. Attempts to remove the loop by increasing the tension can destroy a rod through the process of *hockling* which is described below.

Fig. 1 shows an infinitely long rod with a circular cross section of radius a and made from a linear elastic material with Young's modulus E and Poisson's ratio ν. The rod is initially straight and subject

* Fax: +00-61-7-3365-1477.
E-mail address: dms@maths.up.edu.au (D.M. Stump)

0020-7683/00/$ - see front matter
PII: S0020-7683(99)00019-0

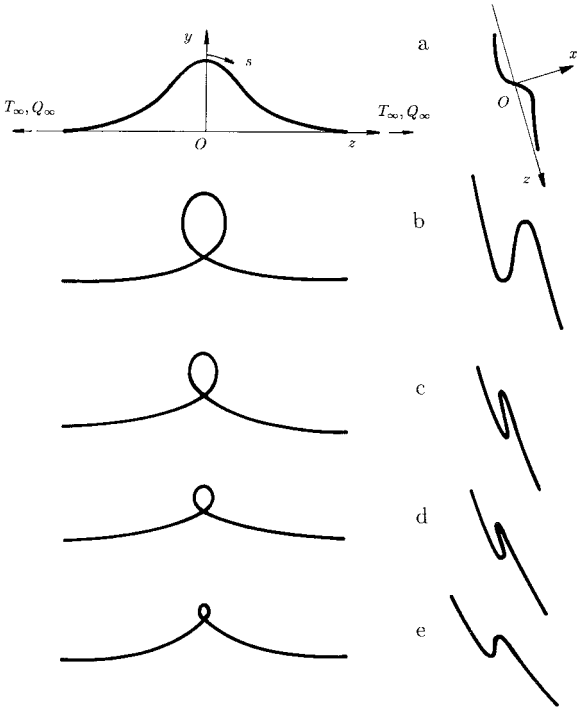

Fig. 1. Side and plan views of the rod centre line for: (a) The Coyne solution in the loading region $\frac{Q_\infty^2}{4} \le T_\infty \le \frac{Q_\infty^2}{2}$. (b) The loading region $\frac{Q_\infty^2}{2} \le T_\infty \le T_c$ prior to side contact. (c) The formation of the contacting loop at $T_\infty = T_c$. (d) The drawing down of the contacting loop in the loading region $T_c \le T_\infty \le T_l$. (e) The pull apart of the contacting loop at the critical tension $T_\infty = T_l$.

to the remote dimensionless tension T_∞ and torque Q_∞ (defined according to the scheme described in Eq. (5)). Greenhill (1883) showed that the rod first buckles when the tension is reduced to the critical value,

$$T_\infty = \frac{Q_\infty^2}{4}.$$

As the remote applied tension T_∞ increases from this level under fixed applied Q_∞, the solution quickly localises into a form similar to a solitary wave solution (Coyne, 1990), see Fig. 1(a). For $T_\infty > Q_\infty^2/2$, the rod shows the appearance of a loop when viewed from the side, Fig. 1(b). At first, the loop is *noncontacting*, that is the sides of rod surface do not rub together. However, as T_∞ increases to a critical value $T_\infty = T_c$, a *contacting* loop is formed when the sides touch each other at some distance along the axis running through the centre of the rod [Fig. 1(c)]. As T_∞ is further increased, the contacting loop is drawn down in size [Fig. 1(d)] until, at a second critical tension $T_\infty = T_l$, the surfaces of the rod pull away (i.e. lift off) from each other to produce a very small loop [Fig. 1(e)]. The small radius of curvature of this second noncontacting loop produces large local strains which can permanently deform (hockle) a metal or fibre-optic cable in this region.

The theory of elastic rods is used to describe the process of hockling shown in Fig. 1. This theory has a long history, much of which is summarised in Chapter 18 in the treatise by Love (1927) and in the recent volume by Antman (1995). There have been a number of analyses of localised rod shapes with the context of undersea cable laying. The most pertinent theoretical work is that of Coyne (1990), who first obtained a closed form solution for the localised mode in an infinitely long inextensible and

unshearable rod and also estimated the tension T_∞ and torque Q_∞ combinations associated with the formation of contacting solutions. Dwivedi et al. (1990) have used a simple planar bending model to treat the case of no remote applied twisting moment. Champneys and Thompson (1996) and Thompson and Champneys (1996) have studied localised mode shapes in inextensible and unshearable rods with linear and nonlinear constitutive laws along with nonisotropic cross-sectional properties, but they have not considered the development of contacting solutions.

There have been several recent applications of the theory beams and rods that undergo extensional and shear deformations in addition to bending and twist. Libai (1992) and Goto et al. (1990) have incoporated these effects into the planar equations for the large kinematic deformation of the bent beam and have studied various planar problems. Champneys et al. (1997) have also considered the development of localised modes in linear elastic rods which undergo shear and extension in addition to bending and twist. Their formulation has also included the effects of: gravity, nonisotropic cross-sectional properties; and initial curvature. Importantly, the neglect of these three effects produces a system of equations which is completely integrable so that no spatially chaotic solutions, such as those described by Mielke and Holmes (1988), are observed.

This study applies a rod theory which incorporates shear and extensible deformations as well as bending and twisting curvatures to the analysis of the hockling problem shown in Fig. 1 in order to find the localised shape, forces, and moments within the rod for various values of T_∞ and Q_∞. The study is organised as follows. In Section 2, the mathematical formulation of the problem is described in terms of both a global vector system and a material-based vector system that is fixed to the central axis of the rod. In Section 3, the equations governing the forces and moments within the rod are integrated to obtain a new closed form solution for this formulation. (This solution reduces to the Coyne (1990) solution in the limit of an unshearable and inextensible rod.) In Section 4, this new solution is used to determine the T_∞ and Q_∞ combinations associated with the formation of the contacting and lift-off solutions shown in Fig. 1. The prediction of the loop shape during the drawing down process shown in Fig. 1(c) is beyond the scope of this study. The results are compared with predictions made by the simpler inextensible and unshearable beam model, and the inclusion of shear and extension deformations is seen to alter significantly the small loop results. Section 5 closes this study with some concluding remarks on the applicability of the results.

2. Mathematical formulation

When an elastic structure has an elongated shape in one direction it is often modelled with a subset of the general equations of elasticity known as a rod theory. Since various simplifying assumptions go into the formulation of a rod theory, there are a number of different approaches depending upon the degree of approximation desired. The simplest set of equations are those of the Kirchoff–Clebsch theory for the *elastica*, which is a rod that can be bent and twisted but is inextensible and unshearable. A more complicated approach allows the elements of the rod to undergo extensional and transverse shear deformations. A detailed discussion of the origin of various rod theories and the assumptions behind their approximations can be found in Antman (1995).

The choice of which rod theory to use depends upon the problem under consideration. When the strains due to the tangential and transverse forces acting on the material element are all 'small' compared to those due to bending and twisting, and plane cross sections remain perpendicular to the centreline of the beam, the elastica model is often accurate enough. However, when these assumption are violated, the shear and extensional deformations may be important in the modelling and a more complex model is appropriate. This is conjectured to be the case for the elastic rod at the lift-off condition shown in Fig. 1(d). The small curvature of the loop relative to the rod radius and the large

tensile and shear forces produce strains which are significant with respect to those due to bending and twisting alone, while plane sections of the rod do not remain perpendicular to the centreline of the rod. The incorporation of these effects is important to improve the accuracy of the results.

In order to obtain an integrable system of equations, the rod is assumed to be linear elastic and to have a circular cross-section of radius a. The natural state of the rod is taken as a straight cylinder. Throughout this study dimensionless quantities defined in Eq. (5) below are employed. The characteristic length and the force-like quantity are taken, respectively, as the rod radius a and the bending rigidity $B = EI$ ($I = \pi a^4/4$ is the second moment of area for a circular rod).

2.1. The coordinate systems and governing equations

The shape of the infinite rod shown in Fig. 1 has a single localised loop which is described in terms of a Cartesian axes system $Oxyz$ with the unit basis vectors (**i**, **j**, **k**). The location of the origin O is chosen so that the **k** axis lies along the line of remote loading and the rod shape is symmetric in the z-coordinate. The rod is parameterised by an *undeformed* arc-length coordinate s which is measured from the point at the top of the *deformed* loop. Because of symmetry only the half-interval $0 \leq s < \infty$ needs to be considered. The location in space of points along the central axis of the rod is described by the position vector $\mathbf{r}(s)$.

Affixed to each material element in the reference configuration is a system of unit vectors ($\mathbf{d}_1$, $\mathbf{d}_2$, $\mathbf{d}_3$) which change orientation with the deformation of the material. The unit vector $\mathbf{d}_3$ points in the directon perpendicular to the cross section of the rod, and the vectors ($\mathbf{d}_1$, $\mathbf{d}_2$) span the cross-sectional plane, see Fig. 2. Because only a circular cross-section rod fashioned from a uniform material is considered here, the initial choice for the orientation of ($\mathbf{d}_1$, $\mathbf{d}_2$) is arbitrary. (This would not be the case in a rod with nonisotropic cross-sectional properties.) The presence of shear strains between the material elements along the rod means that the vector $\mathbf{d}_3$ does *not* point in the direction tangent to the path of the centreline path $\mathbf{r}(s)$.

2.1.1. The equilibrium equations

The forces and moments acting through the center of the rod cross section, shown in Fig. 2, are

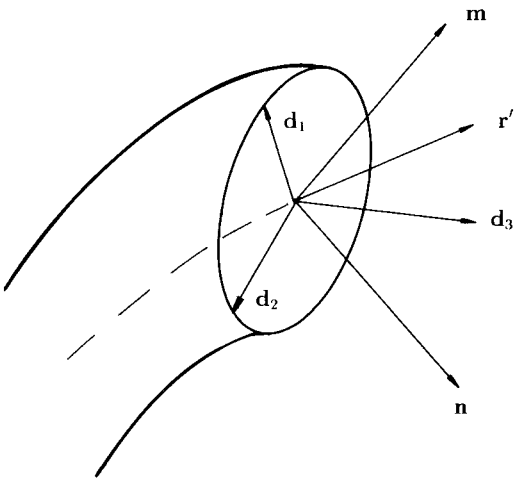

Fig. 2. A schematic drawing of a rod cross section showing the material vector system ($\mathbf{d}_1$, $\mathbf{d}_2$, $\mathbf{d}_3$), the tangent to the centre line $\mathbf{r}'$, along with the force and moment vectors **n** and **m**.

described by the vectors **n** and **m**, respectively (in the notation of Champneys et al., 1997). These vectors can be expressed in either the material or Cartesian vector systems by:

$$\mathbf{n} = n_1\mathbf{d}_1 + n_2\mathbf{d}_2 + n_3\mathbf{d}_3 = n_x\mathbf{i} + n_y\mathbf{j} + n_z\mathbf{k}$$

$$\mathbf{m} = m_1\mathbf{d}_1 + m_2\mathbf{d}_2 + m_3\mathbf{d}_3 = m_x\mathbf{i} + m_y\mathbf{j} + m_z\mathbf{k},$$

where the subscripts (1, 2, 3) are used to denote quantities projected in the material coordinate system at a particular point along the rod; and the subscripts (x, y, z) denote the components of the same vector projected in the Cartesian coordinate system. The forces (n_1, n_2) are shear forces, and n_3 is a tensile force. The moments (m_1, m_2) are bending moments, and m_3 is a twisting moment.

The enforcement of translational and rotational moment equilibrium of the elements of the rod, which is free from any lateral applied loads or couples, gives the two vector equations,

$$\mathbf{n}' = \mathbf{0}, \tag{1a}$$

$$\mathbf{m}' + \mathbf{r}' \wedge \mathbf{n} = \mathbf{0}. \tag{1b}$$

2.1.2. The kinematics

The deformation of the rod is described in terms of the curvature vector **u** and the strain vector **v**, both of which can also be projected into either set of coordinates. The components (u_1, u_2) are bending curvatures, and u_3 is a twisting curvature. Similarly, the strain vector components (v_1, v_2) are transverse shear strains, and v_3 is a tangential strain.

The evolution of the material vector system along the rod is expressed by the vector equations $\mathbf{d}_i' = \mathbf{u} \wedge \mathbf{d}_i$, where $i = (1, 2, 3)$ and the notation $()'$ denotes differentiation with respect to the coordinate s. When written out, these three vector equations have the form:

$$\mathbf{d}_1{}' = u_3\mathbf{d}_2 - u_2\mathbf{d}_3, \quad \mathbf{d}_2{}' = u_1\mathbf{d}_3 - u_3\mathbf{d}_1, \quad \mathbf{d}_3{}' = u_2\mathbf{d}_1 - u_1\mathbf{d}_2. \tag{2}$$

The position vector **r** is related to the strain vector **v** and $\mathbf{d}_3$ by the formula,

$$\mathbf{r}' = \mathbf{v} + \mathbf{d}_3. \tag{3}$$

Once **u** and **v** have been determined along the rod, the material vectors $\mathbf{d}_i$ and the shape vector **r** are found from Eqs. (2) and (3).

2.1.3. The constitutive laws

The specification of the governing equations is completed with constitutive laws which relate the moments **m** with the curvatures **u** and the forces **n** with the strains **v**. In vector dyadic notation, these relationships are given by:

$$\mathbf{n} = (C\mathbf{d}_1\mathbf{d}_1 + C\mathbf{d}_2\mathbf{d}_2 + D\mathbf{d}_3\mathbf{d}_3) \cdot \mathbf{v}, \tag{4a}$$

$$\mathbf{m} = (\mathbf{d}_1\mathbf{d}_1 + \mathbf{d}_2\mathbf{d}_2 + K\mathbf{d}_3\mathbf{d}_3) \cdot \mathbf{u}, \tag{4b}$$

where K, D, and C are, respectively, the *dimensionless* torsional, extensional, and shear rigidities defined in Eq. (5). It is worth noting that since the bending rigidity $B = EI$ has been used in the nondimensionalisation, the modulus drops out of the first two terms on the right side of Eq. (4b). In terms of dimensional quantities (denoted by an overbar), $\bar{K} = GJ$ and $\bar{D} = EA$ where G is the shear

modulus, $J=\pi a^2/2$ is the polar moment of inertia and $A=\pi a^2$ is the cross-sectional area. The modulus $\bar{C}=q\bar{D}$ is an approximation (Fung, 1965) which depends upon the cross-sectional shape. For a circular rod, the value $q = 5/6$ is often used. An inextensible and unshearable rod theory is obtained from the limit $(D,C)\to\infty$, in which case, $\mathbf{n}$ is found from equilibrium considerations; the inversion of Eq. (4a) gives $\mathbf{v}=\mathbf{0}$; and Eq. (3) becomes $\mathbf{r}'=\mathbf{d}_3$.

It should be pointed out that no account of the effects of changes in the cross-sectional dimensions on the constitutive relations of the rod is included in this formulation. Similarly, warping is neglected so that plane sections of the rod are assumed to remain plane, but not perpendicular, to the centre line.

2.1.4. The dimensionless variables

The complete set of equations for the eight dimensionless vector quantities ($\mathbf{r}$, $\mathbf{u}$, $\mathbf{v}$, $\mathbf{n}$, $\mathbf{m}$, $\mathbf{d}_1$, $\mathbf{d}_2$, $\mathbf{d}_3$) is given by Eqs. (1–4). Following the analysis of Fraser and Stump (1998), the various dimensionless quantities used in the analysis are related to the physical (barred) quantities by the formulae:

$$\left.\begin{aligned} &s=\frac{\bar{s}}{a}, \quad \mathbf{r}=\frac{\bar{\mathbf{r}}}{a}, \quad \mathbf{m}=\frac{\bar{\mathbf{m}}a}{B}, \quad \mathbf{n}=\frac{\bar{\mathbf{n}}a^2}{B},\\ &\mathbf{u}=\bar{\mathbf{u}}a, \quad K=\frac{\bar{K}}{B}, \quad D=\frac{\bar{D}a^2}{B}, \quad C=\frac{\bar{C}a^2}{B}, \end{aligned}\right\} \tag{5}$$

The strain vector $\mathbf{v}$ is dimensionless by definition. It is important to note that in this normalisation scheme, the values of the elastic constants for a circular rod are given by the $O(1)$ quantities:

$$K=\frac{1}{1+\nu}, \quad D=4, \quad C=q4.$$

The magnitude of the force and moment vectors $\mathbf{n}$ and $\mathbf{m}$ are typically much smaller than $O(1)$ so that the strains within the rod elements do not exceed the material's elastic limit.

This normalisation scheme is different from that used by other studies (e.g. Champneys et al., 1997) where the magnitudes of the dimensionless $\mathbf{n}$ and $\mathbf{m}$ are both $O(1)$. That approach leads to dimensionless shear and extensional rigidities which are much smaller than the dimensionless bending and torsional rigidities. The results of either normalisation scheme can be shown to be equivalent.

2.2. Euler angles and boundary conditions

In order to integrate the governing equations Eqs. (1–4), a suitable set of boundary conditions is necessary. In terms of the global Cartesian vector system aligned so that the $\mathbf{k}$-axis points along the line of remote applied loading, the remote conditions as $s\to\infty$ are:

$$\mathbf{r}\sim\left(1+\frac{T_\infty}{D}\right)s\mathbf{k}, \quad \mathbf{d}_3\sim\mathbf{k}, \quad \mathbf{n}\sim T_\infty\mathbf{k}, \quad \mathbf{m}\sim Q_\infty\mathbf{k}. \tag{6}$$

The remote values of $\mathbf{u}$ and $\mathbf{v}$ are obtained from the constitutive laws (Eqs. (4a) and (4b)).

The governing equations are most naturally integrated in terms of their components in the material vector system ($\mathbf{d}_1$, $\mathbf{d}_2$, $\mathbf{d}_3$) while the boundary conditions are expressed in terms of the global Cartesian system ($\mathbf{i}$, $\mathbf{j}$, $\mathbf{k}$). The connection between the two vector systems is provided by the Euler angles (θ, ϕ, ψ) which are functions of the material coordinate s.

In the notation of Landau and Lifshitz (1963) [p. 110], Fig. 3 shows the definitions of the angles (θ, ϕ, ψ) in relation to the two sets of orthogonal axes. A geometrical analysis of Fig. 3 leads to the trigonometric formulae:

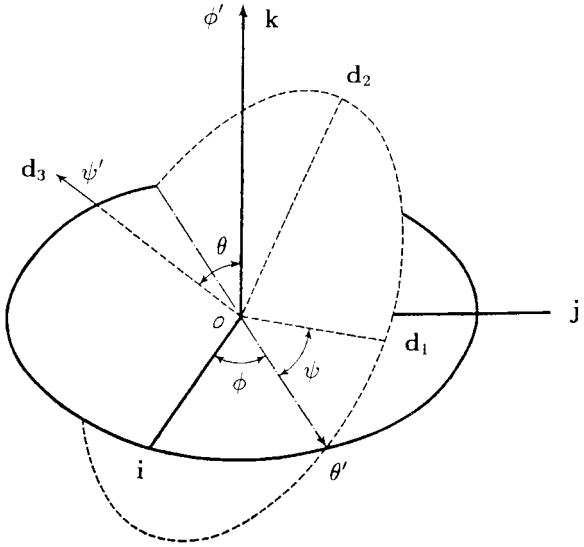

Fig. 3. A schematic drawing showing the relationship between the Cartesian basis vectors (**i**, **j**, **k**) and the material basis vectors ($\mathbf{d}_1$, $\mathbf{d}_2$, $\mathbf{d}_3$) along with the Euler angles (θ, ϕ, ψ) and their derivatives.

$$\mathbf{d}_1 = (\cos\psi\cos\phi - \sin\psi\cos\theta\sin\phi)\mathbf{i} + (\cos\psi\sin\phi + \sin\psi\cos\theta\cos\phi)\mathbf{j} + \sin\psi\sin\theta\mathbf{k},$$

$$\mathbf{d}_2 = -(\sin\psi\cos\phi + \cos\psi\cos\theta\sin\phi)\mathbf{i} + (-\sin\psi\sin\phi + \cos\psi\cos\theta\cos\phi)\mathbf{j} + \cos\psi\sin\theta\mathbf{k},$$

$$\mathbf{d}_3 = \sin\theta\sin\phi\mathbf{i} - \sin\theta\cos\phi\mathbf{j} + \cos\theta\mathbf{k}, \tag{7}$$

connecting the two systems of basis vectors. By projecting the rates of rotation of the Euler angles (θ', ϕ', ψ') along the axes ($\mathbf{d}_1$, $\mathbf{d}_2$, $\mathbf{d}_3$) and using the evolution equations Eq. (2), it is straightforward to relate the components of the curvature vector **u** to the derivatives (θ', ϕ', ψ') via

$$\theta' = u_1\cos\psi - u_2\sin\psi, \tag{8a}$$

$$\phi' = \frac{u_1\sin\psi + u_2\cos\psi}{\sin\theta}, \tag{8b}$$

$$\psi' = u_3 - \phi'\cos\theta. \tag{8c}$$

Once the compenents of **u** have been found, these equations can, in principle, be integrated to obtain the Euler angles as a function of position along the rod. However, as is shown below, an alternative approach provides the angles θ and ψ directly without the need to integrate Eqs. (8a) and (8c). The angle ϕ is obtained from a trivial integration of Eq. (8b). Care needs to be exercised in the use of Eqs. (8a), (8b) and (8c) for general problems due to the polar singularity in Eq. (8b). A phase plane analysis is used below to show that the localised solution found here corresponds to a homoclinic orbit that does not pass through the singularity.

3. Integration of the equations

The governing equations are integrated to obtain the various quantities within the rod and to find the position vector **r** within the global Cartesian reference axes. The starting point of the analysis is the equilibrium equations (Eqs. (1a) and (1b)), which are integrated in both the Cartesian and material vector systems.

3.1. The Cartesian representation

In the Cartesian representation, the integration of Eq. (1a) with the remote boundary conditions gives the constant vector,

$$\mathbf{n} = n_x\mathbf{i} + n_y\mathbf{j} + n_z\mathbf{k} = T_\infty\mathbf{k}. \tag{9}$$

This expression is inserted into Eq. (1b) which is then integrated to obtain the Cartesian form:

$$\mathbf{m} = m_x\mathbf{i} + m_y\mathbf{j} + m_z\mathbf{k} = Q_\infty\mathbf{k} - \mathbf{r} \wedge T_\infty\mathbf{k}. \tag{10}$$

These expressions are used below to find the shape of the rod.

3.2. The material vector representation

An alternative integration of the governing equations can be done by expressing the various quantities in the material vector system ($\mathbf{d}_1$, $\mathbf{d}_2$, $\mathbf{d}_3$). It is straightforward to show that the equilibrium equations (Eqs. (1a) and (1b)) take the expanded forms:

$$n_1'\mathbf{d}_1 + n_2'\mathbf{d}_2 + n_3'\mathbf{d}_3 + n_1\mathbf{d}_1' + n_2\mathbf{d}_2' + n_3\mathbf{d}_3' = \mathbf{0}, \tag{11a}$$

$$m_1'\mathbf{d}_1 + m_2'\mathbf{d}_2 + m_3'\mathbf{d}_3 + m_1\mathbf{d}_1' + m_2\mathbf{d}_2' + m_3\mathbf{d}_3' + [v_1\mathbf{d}_1 + v_2\mathbf{d}_2 + (1+v_3)\mathbf{d}_3] \wedge [n_1\mathbf{d}_1 + n_2\mathbf{d}_2 + n_3\mathbf{d}_3] = \mathbf{0}. \tag{11b}$$

Use of the definitions Eq. (2) for the vector derivatives $\mathbf{d}_i'$ and the constitutive relationships,

$$n_1 = Cv_1, \quad n_2 = Cv_2, \quad n_3 = Dv_3, \quad m_1 = u_1, \quad m_2 = u_2, \quad m_3 = Ku_3 \tag{12}$$

provided by Eqs. (4a) and (4b) allows Eqs. (11a) and (11b) to be written out as the six equations:

$$n_1' = \frac{1}{K}m_3n_2 - n_3m_2, \tag{13a}$$

$$n_2' = m_1n_3 - \frac{1}{K}m_3n_1, \tag{13b}$$

$$n_3' = m_2n_1 - m_1n_2, \tag{13c}$$

$$m_1' = \left(\frac{1}{K} - 1\right)m_3m_2 - \frac{1}{C}n_2n_3 + n_2\left(1 + \frac{n_3}{D}\right), \tag{13d}$$

$$m_2{}' = \left(1 - \frac{1}{K}\right) m_3 m_1 + \frac{1}{C} n_1 n_3 - n_1 \left(1 + \frac{n_3}{D}\right), \tag{13e}$$

$$m_3{}' = 0, \tag{13f}$$

for the components of **n** and **m**.

3.2.1. Integration of the equations

The nonlinear equations (Eqs. (13a), (13b), (13c), (13d), (13e) and (13f)) are integrated in conjunction with the remote boundary conditions (6) as follows:

1. Eq. (13f) is integrated immediately to get

$$m_3 = Q_\infty. \tag{14}$$

2. The combination of Eqs. (13a), (13b) and (13c) gives

$$n_1 n_1{}' + n_2 n_2{}' + n_3 n_3{}' = 0,$$

which is integrated to obtain

$$n_1^2 + n_2^2 + n_3^2 = T_\infty^2. \tag{15}$$

3. The combination of Eqs. (13a), (13b), (13c), (13d), (13e) and (13f) gives

$$m_1 n_1{}' + n_1 m_1{}' + m_2 n_2{}' + n_2 m_2{}' + m_3 n_3{}' = 0,$$

which is integrated to get

$$n_1 m_1 + n_2 m_2 + n_3 m_3 = T_\infty Q_\infty. \tag{16}$$

4. The combination of Eqs. (13d) and (13e) yields

$$m_1 m_1{}' + m_2 m_2{}' = -n_3{}'(1 - k n_3),$$

where the constant k is given by

$$k = \frac{D - C}{DC}.$$

(Under this normalisation scheme, $k \sim 1/20$ for a circular cross-section rod with $q = 5/6$.) This equation is integrated to obtain

$$\frac{1}{2} m_1^2 + \frac{1}{2} m_2^2 = (T_\infty - n_3) - \frac{k}{2}\left(T_\infty^2 - n_3^2\right). \tag{17}$$

5. The combination of Eqs. (13a) and (13b) gives

$$n_2 n_1{}' - n_1 n_2{}' = \frac{1}{K} m_3 \left(n_1^2 + n_2^2\right) - n_3 (m_1 n_1 + m_2 n_2).$$

This expression is divided by $n_1^2 + n_2^2$ and use is made of Eqs. (14)–(16) to obtain the differential equation,

$$-\left[\tan^{-1}\left(\frac{n_2}{n_1}\right)\right]' = \frac{Q_\infty}{K} - \frac{Q_\infty n_3}{T_\infty + n_3}. \tag{18}$$

6. The system of equations has now been reduced to Eqs. (14)–(17) and the two differential equations Eqs. (13c) and (18). The introduction of the auxiliary variables (ρ, γ, r, α) defined by:

$$n_1 = \rho\cos\gamma, \quad n_2 = \rho\sin\gamma, \quad m_1 = r\cos\alpha \quad \text{and} \quad m_2 = r\sin\alpha,$$

allows the set of equations to be transformed into

$$m_3 = Q_\infty, \tag{19a}$$

$$\rho^2 + n_3^2 = T_\infty^2, \tag{19b}$$

$$\rho r\cos(\gamma - \alpha) + n_3 Q_\infty = T_\infty Q_\infty, \tag{19c}$$

$$\frac{r^2}{2} = (T_\infty - n_3) - \frac{k}{2}\left(T_\infty^2 - n_3^2\right), \tag{19d}$$

$$\gamma' = -\frac{Q_\infty}{K} + \frac{Q_\infty n_3}{T_\infty + n_3}, \tag{19e}$$

$$n_3' = -\rho r\sin(\gamma - \alpha). \tag{19f}$$

7. An equation for n_3 is obtained by combining Eqs. (19c) and (19f) to get

$$\rho^2 r^2 = \left(n_3'\right)^2 + (T_\infty - n_3)^2 Q_\infty^2,$$

and also by combining Eqs. (19b) and (19d) to yield

$$\rho^2 r^2 = \left(T_\infty^2 - n_3^2\right)\left[2(T_\infty - n_3) - k\left(T_\infty^2 - n_3^2\right)\right].$$

These expressions are equated and simplified to provide the first order differential equation for n_3,

$$n_3' = (T_\infty - n_3)\left[2(T_\infty + n_3) - k(T_\infty + n_3)^2 - Q_\infty^2\right]^{1/2}. \tag{20}$$

where the positive square root has been taken since for $s \geq 0$, n_3 is a monotonically increasing function. Eq. (20) is integrated in the Appendix and is given by the closed-form expression:

$$n_3 = T_\infty - \frac{\sqrt{\Delta}e^{\sqrt{c}s}}{\frac{1}{4c}\left[\sqrt{\Delta}e^{\sqrt{c}s} - b\right]^2 + k}, \tag{21}$$

where the terms b and c represent the variable combinations,

$$b = -2(1 - 2kT_\infty); \quad c = 4T_\infty - Q_\infty^2 - 4kT_\infty^2, \quad \text{and} \quad \Delta = b^2 + L/kc.$$

The value of $b \leq -2$, and it is expected that $c \geq 0$ for the values $T_\infty \leq O(1)$, which are reasonable under this normalisation.

8. Eq. (21) is inserted into Eq. (19e) which is factored into the differential equation

$$\gamma' = Q_\infty\left(\frac{1}{2} - \frac{1}{\kappa}\right) - \frac{Q_\infty\sqrt{\Delta}e^{\sqrt{c}s}}{\dfrac{T_\infty}{c}\left(\sqrt{\Delta}e^{\sqrt{c}s} - b\right)^2 + 4kT_\infty - 2\sqrt{\Delta}e^{\sqrt{c}s}}. \tag{22}$$

This equation is integrated (Gradstyn and Ryzhik, 1965) to obtain

$$\gamma' = Q_\infty\left(\frac{1}{2} - \frac{1}{\kappa}\right)s - \frac{Q_\infty}{\sqrt{16k2T_\infty^2 + Q_\infty^2}}\tan^{-1}\left[\frac{(\beta = 2\alpha\sqrt{\Delta})(e^{\sqrt{c}s} - 1)\sqrt{\Lambda}}{\Lambda + (\beta = 2\alpha\sqrt{\Delta})^2 e^{\sqrt{c}s}}\right], \tag{23}$$

where

$$\alpha = \frac{T_\infty}{c}, \quad \beta = -2\left(1 + \frac{T_\infty b}{c}\right), \quad \text{and} \quad \Lambda = \frac{16T_\infty}{c}\left(1 + 3kT_\infty\right) - 4.$$

In general it is expected that $\beta \leq 0$ since, for $k \sim 1/20$, $\beta \leq 0$ for values of $T_\infty \leq 6.667$, which includes all practical cases.

The integration of Eqs. (13a), (13b), (13c), (13d), (13e) and (13f) is now complete and the components of **n** and **m** are found by back substitution.

3.3. The Euler angles

The three Euler angles (θ, ϕ, ψ) are now calculated. The force vector **n** given by Eq. (9) has the two equivalent representations,

$$\mathbf{n} = \rho\cos\gamma\mathbf{d}_1 + \rho\sin\gamma\mathbf{d}_2 + n_3\mathbf{d}_3 = T_\infty\mathbf{k}, \tag{24}$$

where the auxiliary variables (ρ, γ) have been used in place of (n_1, n_2). The formation of successive dot products of Eq. (24) with each of the basis vectors ($\mathbf{d}_1$, $\mathbf{d}_2$, $\mathbf{d}_3$) and use of Eq. (7) gives:

$$\rho\cos\gamma = T_\infty\sin\psi\sin\theta, \quad \rho\sin\gamma = T_\infty\cos\psi\sin\theta, \quad n_3 = T_\infty\cos\theta.$$

This set of equations yields formulae for the two Euler angles θ and ψ,

$$\theta = \cos^{-1}\left(\frac{n_3}{T_\infty}\right) \tag{25a}$$

$$\psi = \frac{\pi}{2} - \gamma, \tag{25b}$$

without the need to integrate Eqs. (8a) and (8c). The angle ϕ is determined by using the results for ψ and θ and the constitutive relations Eq. (12) to transform (8b) into

$$\phi' = \frac{m_1\cos\gamma + m_2\sin\gamma}{\sqrt{1 - \dfrac{n_3^2}{T_\infty^2}}}.$$

The introduction of the formulae $m_1 = r\cos\alpha$ and $m_2 = r\sin\alpha$ provides

$$\phi' = \frac{r\cos(\gamma-\alpha)}{\sqrt{1-\dfrac{n_3^2}{T_\infty^2}}} = \frac{Q_\infty T_\infty}{T_\infty + n_3},$$

where the right-most expression has been obtained by using various relations (Eqs. (19a), (19b), (19c), (19d), (19e) and (19f)). The addition of this expression and Eq. (19e) gives

$$\phi' + \gamma' = Q_\infty\left(1-\frac{1}{K}\right),$$

which is trivially integrated (the constant of integration being set equal to zero) to obtain the formula

$$\phi = Q_\infty\left(1-\frac{1}{K}\right)s - \gamma \tag{26}$$

for the final Euler angle. A check on the solution is provided by taking the limit $s \to \infty$, in which case, Eqs. (21) and (23) give

$$n_3 \sim T_\infty, \quad \gamma \sim Q_\infty\left(\frac{1}{2}-\frac{1}{K}\right)s,$$

which leads to the asymptotic Euler angles:

$$\theta \sim 0, \quad \psi \sim Q_\infty\left(\frac{1}{K}-\frac{1}{2}\right)s, \quad \phi \sim \frac{Q_\infty s}{2}.$$

From Fig. 3, it can be seen that as $\theta \to 0$, ϕ and ψ are coplanar and the sum $\phi+\psi \sim Q_\infty s/K$ gives the total twist about the **k**-axis. In addition, the asymptotic form of Eq. (8c) provides the rate of twist,

$$u_3 \sim \psi' + \phi' = \frac{Q_\infty}{K},$$

which is the correct formula for the rate of twist of a straight rod under the remote torque Q_∞.

3.4. The tangent and position vectors

The results obtained so far are now used to find the tangent and position vectors as functions of s.

3.4.1. The tangent vector

From Eq. (3) and the constitutive laws Eq. (12), the Cartesian form of the tangent vector can be expressed as

$$x'\mathbf{i} + y'\mathbf{j} + z'\mathbf{k} = \frac{\rho}{C}\cos\gamma\,\mathbf{d}_1 + \frac{\rho}{C}\sin\gamma\,\mathbf{d}_2 + \left(1+\frac{n_3}{D}\right)\mathbf{d}_3. \tag{27}$$

The formation of the scalar product of Eq. (27) with each of (**i**, **j**, **k**) along with the use of Eq. (7), various trigonometric identities, and $\psi+\gamma=\pi/2$ leads to the component expressions

$$x' = -\frac{\rho}{C}\cos\theta\sin\phi + \left(1+\frac{n_3}{D}\right)\sin\theta\sin\phi, \tag{28a}$$

$$y' = \frac{\rho}{C}\cos\theta\cos\phi - \left(1+\frac{n_3}{D}\right)\sin\theta\cos\phi, \tag{28b}$$

$$z' = \frac{\rho}{C}\sin\theta + \left(1+\frac{n_3}{D}\right)\cos\theta. \tag{28c}$$

In the inextensible and unshearable limit $(D,C)\to\infty$, the Eqs. (28a), (28b) and (28c) reduce to

$$x' = \sin\theta\sin\phi; \quad y' = -\sin\theta\cos\phi; \quad z' = \cos\theta,$$

which agrees with Love (1927) [Chapter 18].

3.4.2. The position vector

The formation of the vector product of **k** with Eq. (10) and use of the triple vector product leads to the formula

$$T_\infty(x\mathbf{i}+y\mathbf{j}) = m_y\mathbf{i} - m_x\mathbf{j}.$$

The use of the expressions $m_x = \mathbf{m}\cdot\mathbf{i}$ and $m_y = \mathbf{m}\cdot\mathbf{j}$ allows this equation to be separted into the components

$$x = \frac{1}{T_\infty}\mathbf{j}\cdot[m_1\mathbf{d}_1 + m_2\mathbf{d}_2 + m_3\mathbf{d}_3], \quad y = -\frac{1}{T_\infty}\mathbf{i}\cdot[m_1\mathbf{d}_1 + m_2\mathbf{d}_2 + m_3\mathbf{d}_3].$$

The expansion of the dot products according to Eq. (7) and the use of various trigonometric identities provide the final formulae:

$$x = \frac{r}{T_\infty}\sin\phi\cos(\alpha+\psi) + \frac{r}{T_\infty}\cos\theta\cos\phi\sin(\alpha+\psi) - \frac{Q_\infty}{T_\infty}\sin\theta\cos\phi, \tag{29a}$$

$$y = -\frac{r}{T_\infty}\cos\phi\cos(\alpha+\psi) + \frac{r}{T_\infty}\cos\theta\sin\phi\sin(\alpha+\psi) - \frac{Q_\infty}{T_\infty}\sin\theta\sin\phi. \tag{29b}$$

The z-component of the position vector must be obtained from the integration of Eq. (28c), which yields the formula

$$z = \left(1+\frac{T_\infty}{D}\right)s + \frac{2\sqrt{c}}{T_\infty}\left(\frac{\sqrt{\Delta} - be^{\sqrt{c}s}}{\sqrt{\Delta}(1+e^{2\sqrt{c}s}) - 2be^{\sqrt{c}s}} - \frac{1}{2}\right). \tag{30}$$

This completes the solution for the shape of the shearable and extensible rod. It can be shown that in the inextensible and unshearable limit $(C,D)\to\infty$, the analytical expressions obtained here reduce to the corresponding expressions found by Coyne (1990).

3.5. Phase plane analogy

Since the rod equations are completely integrable, the phase plane constructed for θ and θ' is a useful tool to show that the localised solution found here represents a homoclinic orbit and that the polar singularity associated with $\theta = 0$ is avoided. The phase plane is constructed by replacing $n_3 = T_\infty\cos\theta$ in Eq. (21) and then rewriting this equation in the form:

$$\frac{1}{2}\theta'^2 + V(\theta) = T_\infty - kT_\infty^2, \tag{31}$$

where

$$V(\theta) = \frac{Q_\infty^2}{2}\left(\frac{1-\cos\theta}{1+\cos\theta}\right) + T_\infty\cos\theta - \frac{kT_\infty^2}{2}\cos^2\theta. \tag{32}$$

The equation of a nonlinear oscillator is found by taking the derivative of Eq. (31) to obtain

$$\theta'' + \frac{\partial V}{\partial\theta} = 0,$$

where the differentiation of Eq. (32) provides

$$\frac{\partial V}{\partial\theta} = \frac{\sin\theta}{[1+\cos\theta]^2}\left\{Q_\infty^2 T_\infty(1-kT_\infty\cos\theta)(1+\cos\theta)^2\right\}. \tag{33}$$

The fixed points given by the roots of Eq. (33) which are $\theta=0$ and solutions to the cubic equation,

$$\frac{Q_\infty^2}{T_\infty} = (1-kT_\infty\cos\theta)(1+\cos\theta)^2. \tag{34}$$

These represent, respectively, a straight rod and helices. In the inextensible limit $k\to 0$, Eq. (34) agrees with the results of Champneys and Thompson (1996). The detailed structure of this system is currently under further study, but a plot of the phase plane (Fig. 4) for several configurations of the shearable and extensible rod shows that the localised solution is a homoclinic orbit emerging from the fixed point $\theta=0$. Thus, the polar singularity at $\theta=0$ is never encountered except at the asymptotic ends of the orbit.

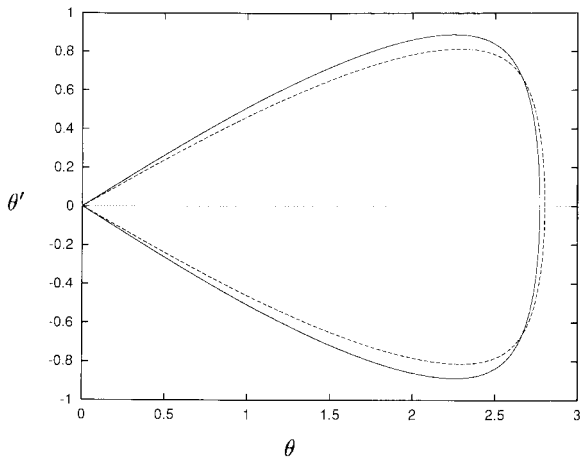

Fig. 4. A phase plane of θ and θ' showing the homoclinic orbits of two localised solutions computed for the values $Q_\infty=0.2$, $K=2/3$, $D=4$, $C=10/3$ and the two values $T_\infty=0.1158$ (solid line) and $T_\infty=0.2452$ (dashed line). These represent the contacting and lift-off solutions, respectively.

4. The contacting and lift-off solutions

The results of the previous section are now used to calculate the loop sizes as measured by $s=L$ (half of the undeformed arc-length in the loop) and the tensions T_∞ associated with the formation of the contacting and lift-off solutions for a rod under fixed remote torque Q_∞. The two sets of solutions for these variables are denoted by (L_c, T_c) for the contacting case and (L_l, T_l) for the lift-off case.

4.1. The equations

There are two conditions that must be enforced to determine L and T_∞. Since the rod shape for $s \le 0$ is obtained by rotating the shape for $s \ge 0$ about the y-axis by 180°, and since the rod material cannot interpenetrate during contact, then at the instant of contact and lift-off the rod centreline must just graze a cylinder of unit radius with the y-axis as generator. This leads to two mathematical conditions. First, the contact point in the xz-plane must lie on the unit circle

$$x(L,T_\infty)^2 + z(L,T_\infty)^2 = 1, \tag{35}$$

where the dependence of the positions components on L and T_∞ is noted explicitly. Second, the projections of the position and tangent vectors in the xz-plane must be perpendicular, that is,

$$x(L,T_\infty)x'(L,T_\infty) + z(L,T_\infty)z'(L,T_\infty) = 0. \tag{36}$$

Eqs. (35) and (36) are two nonlinear conditions for the determination of $s=L$ and T_∞ associated with the contact and lift-off solutions. These must be solved numerically using a Newton–Raphson method (Press et al., 1986) for specified values of the elastic constants (K, D, C) and the remote torque Q_∞.

4.2. Numerical results

The results of calculations for the inextensible and unshearable model $(C,D) \to \infty$ and for the shearable and extensible model ($D = 4$, $C = 10/3$) for an incompressible material $K = 2/3$ are shown in Fig. 5.

Fig. 5(a,b) show, respectively, plots of the loop size L and the tension T_∞ as functions Q_∞. In both figures, the results of the inextensible and unshearable model are given by the solid line, and the results for the shearable and extensible model are shown by the dashed line. It should be noted that the continuum of values $0 \le k \le 0.0503$, (the bounding values correspond to the two sets of data used here) generates a family of curves that are similar in shape to those shown and lie between the two extreme cases. The figures are used to predict the contact and lift-off solutions in the following way. For a specified value of Q_∞, say $Q_\infty = 0.2$, two straight vertical dotted lines are drawn on each plot. Consider first the inextensible and unshearable model and start with a straight rod subject to torque $Q_\infty = 0.2$ and tension T_∞ greater than the Greenhill buckling load. Now start to reduce tension T_∞. The rod buckles at the critical value $T_\infty = 0.01$. In order to form the localised solution, immediately begin to increase T_∞. At the value $T_\infty = 0.02$, a noncontacting loop is seen when the rod is viewed from the side. As T_∞ continues to increase, the vertical line shown on Fig. 5(b) is traversed upwards until the critical value $T_\infty = T_c = 0.1127$ is reached, where the contacting loop has formed. This is associated with the upper intersection point $L_c = 5.54$ where the dotted vertical line cuts the upper side of the solid curve on Fig. 5(a). As T_∞ is further increased, the vertical line in Fig. 5(b) continues to be traversed upwards while the loop is being drawn down in size and the vertical line on Fig. 5(b) is descended. Eventually, the tension reaches the upper intersection point $T_\infty = T_l = 0.2956$ corresponding to the lift-off condition

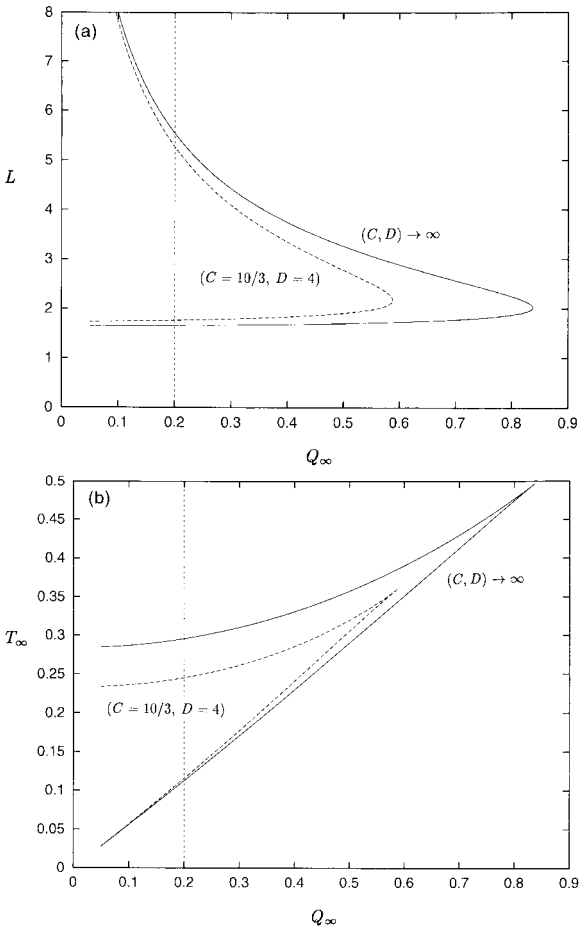

Fig. 5. (a) A plot of the loop size as measured by the material coordinate $s = L$ for the contacting loops (upper branch) and the pull apart loops (lower branch) as functions of the applied remote torque Q_∞. (b) A plot of the remote forces at contact $T_\infty = T_c$ (lower branch) and for pull apart $T_\infty = T_l$ (upper branch) as functions of the applied remote torque Q_∞. In both figures the solid lines show the inextensible and unshearable limit $(C,D) \to \infty$ and $K = 2/3$, while the long dashed lines show the shearable and extensible model results for ($K = 2/3$, $D = 4$ and $C = 10/3$).

when the loop pulls apart. Simultaneously the loop size $L_l = 1.66$ is given by the lower intersection point of the vertical line and the solid curve on Fig. 5(a).

The same imaginary loading process describes the formation of the contacting and lift-off solutions for the shearable and extensible model shown by the dashed lines. However, the critical value of tension T_∞ for the buckling of the shearable rod is found by setting the combination variable c in the formulas of the previous section equal to zero and solving for T_∞. This leads to the critical buckling load T_∞ given by

$$T_\infty = \frac{1 - \sqrt{1 - kQ_\infty^2}}{2k}. \tag{37}$$

With the introduction of the alternative variables

$$m = \frac{Q_\infty}{\sqrt{T_\infty}}, \quad \tilde{k} = kT_\infty,$$

Eq. (37) can be transformed into

$$m = 2\sqrt{1-\tilde{k}},$$

which agrees with the linear eigenvalue results of Champneys et al. (1997) for the governing equations (Eqs. (13a), (13b), (13c), (13d), (13e) and (13f)). Once buckling has occurred and the tension is increased, similar behavior to that discussed above is observed for the formation of contact and lift-off solutions of the shearable and extensible model. Along the example line of $Q_\infty = 0.2$ in Fig. 5, the coordinates of the contact point are $T_c = 0.1158$ and $L_c = 5.27$ and those of the lift-off point are $T_l = 0.2452$ and $L_l = 1.765$. The largest percentage differences between the two models occurs for the lift-off case, which is to be expected since here the additional deformation due to the shear and extension of the rod are significant. For $Q_\infty = 0.20$ the incorporation of shear and extension effects reduces T_l by about 17%. A comparison of the loop sizes at lift-off between the two models is not particularly meaningful since the value L_l describes the material coordinate, which is not the physical arc length for the extensible model.

There is another interesting aspect to the results shown in Fig. 5(a,b). Both models show a maximum torque $Q_\infty = Q_{max}$ beyond which it is not possible to form the contacting solutions. Presumably for $Q_\infty \geq Q_{max}$, the rod is so highly twisted that it cannot displace further than one rod radius away from the remote loading axis and thus never forms a contacting solution. For the inextensible and unshearable model, $Q_{max} \sim 0.84$ while, for the shearable and extensible model, $Q_{max} \sim 0.6$. These are both very large levels of Q_∞, but such a significant reduction in Q_{max} between the two models is surprising.

Most problems of practical interest will involve values of $Q_\infty \leq 0.1$, in which case, a simple leading-order asymptotic analysis of L and T_∞ for the inextensible and unshearable model shows that the contacting solution (L_c, T_c) is given approximately by:

$$L_c \sim \frac{2.55}{\sqrt{Q_\infty}}, \quad T_c \sim 0.555 Q_\infty,$$

while the lift-off solution (L_l, T_l) is given by the constants

$$L_l \sim 1.654, \quad T_l = 0.2839.$$

A similar analysis performed for the shearable and extensible model shows comparable results. The important practical consequence is the result that the loop size at pull apart is essentially independent of Q_∞ for all realistic values of Q_∞. This means that once a loop is formed, it will be virtually impossible not to hockle the cable if the tension is increased monotonically and the loop is drawn down in size. The small size of all the lift-off solutions means that reducing the remote torque Q_∞ prior to drawing down the loop has little effect on the final radius of curvature when the loop is pulled out.

5. Concluding remarks

A new closed-form localised solution for the linear elastic, circular cross-section rod subject to bending, twist, shear, and extensional deformations has been found and agrees with the solution obtained by Coyne (1990) in the inextensible and unshearable limit.

These results are used to predict the contacting and lift-off loops that form in a long rod loaded under remote tension T_∞ and torque Q_∞. The size of the loop at pull out is essentially independent of Q_∞ which means that reducing the remote torque in an attempt to avoid hockling the cable as the tension is increased is unlikely to succeed. The incorporation of shear and extensional deformations in the model modify the small lift-off loop results of the inextensible and unshearable model by about 15%, but do not effect significantly the results for the formation of the contacting loop.

The predicted pull apart loops are very small in size (on the order of four rod radii in length of the undeformed arc-length coordinate) and it is questionable whether any rod theory adequately describes such a large deformation three-dimensional problem. It is felt that the utility of this solution is that it captures the basic trends of results on samples in a small loading rig, and that the closed form nature of the solution allows further exploration of the mathematical features. The development of the solution has also demonstrated how to combine the global Cartesian vector and material vector methods of analysis.

Acknowledgements

This work was supported by an Australian Research Council Large Grant. Helpful discussions with W.B. Fraser, G. van der Heijden, J.M.T. Thompson, and A.R. Champneys have been greatly appreciated. Mr. K. Ma assisted with the some of the calculations.

Appendix. The integration of the n_3-equation

The equation for the component n_3 along the rod is obtained as follows. First, Eq. (20) is integrated to get

$$\int \frac{\mathrm{d}n_3}{(T_\infty - n_3)\sqrt{2(T_\infty + n_3) - k(T_\infty + n_3) - Q_\infty^2]}} = s + c_0,$$

where c_0 is a constant of integration. Next, the variable change

$$\frac{1}{t} = T_\infty - n_3;\ \frac{\mathrm{d}t}{t^2} = \mathrm{d}n_3$$

is made so that the integral is transformed into

$$\int \frac{\mathrm{d}t}{\sqrt{ct^2 + bt - k}} = s + c_0,$$

where the combinations b and c are given by

$$b = -2(1 - 2kT_\infty) \quad \text{and} \quad c = 4T_\infty - Q_\infty^2 - 4kT_\infty^2.$$

Since it is expected that $b \le 0$ and $c \ge 0$, this integral can be evaluated by standard means (Gradstyn and Ryzhik, 1965) to obtain

$$\sqrt{c}\log\left\{2\sqrt{c}(ct^2 + bt - k)^{1/2} + 2ct + b\right\} = s + c_0.$$

This expression is solved for t and the constant c_0 is chosen so that $n_3^1(0) = 0$, which yields the final result Eq. (21). In the inextensible and unshearable limit $(C,D) \to \infty$, the expression for n_3 Eq. (21) reduces to

$$n_3 = T_\infty - \frac{1}{2}(4T_\infty - Q_\infty^2)\operatorname{sech}^2\left(\frac{s}{2}\sqrt{4T_\infty - Q_\infty^2}\right),$$

which agrees with the Coyne (1990) solution.

References

Antman, S.S., 1995. Nonlinear Problems in Elasticity. Springer–Verlag, Berlin.

Champneys, A.R., van der Heijden, G.H.M., Thompson, J.M.T., 1997. Spatially complex localisation after one-twist-per-wave equilibria in twisted circular rods with initial curvature. Phil. Trans. Roy. Soc. Lond. A 355, 2151–2174.

Champneys, A.R., Thompson, J.M.T., 1996. A multiplicity of localised buckling modes. Proc. Roy. Soc. Lond. A 452, 2467–2491.

Coyne, J., 1990. Analysis of the formation and elimination of loops in twisted cable. IEEE J. Oceanic Eng. 15, 72–83.

Dwivedi, J.P., Das Talukar, N.K., Mahmood, N.A., 1990. Mechanics of kinking cables. J. of Eng. Ind. 112, 302–305.

Fraser, W.B., Stump, D.M., 1998. The equilibrium of the convergence point in two-strand yarn plying. Int. J. Solids Structures 35, 285–298.

Fung, Y.C., 1965. In: Foundations of Solid Mechanics. Prentice–Hall, London, pp. 322–324.

Goto, Y., Tomoo, Y., Obata, M., 1990. Elliptic integral solutions of plane elastic with axial and shear deformations. Int. J. Solids Structures 26, 375–390.

Gradstyn, I.S., Ryzhik, I.M., 1965. Tables of Integrals, Series, and Products. Academic Press, New York.

Greenhill, A.G., 1883. On the strength of shafting when exposed both to torsion and end thrust. In: Inst. Mech. Engineers, Proc. 1883, pp. 182–209.

Landau, L.D., Lifshitz,]E.M., 1963. In: Mechanics. Pergamon, Oxford, pp. 105–115.

Libai, A., 1992. Equations for the nonlinear planar deformation of beams. J. App. Mech. 59, 1028–1030.

Love, A.E.H., 1927. In: A Treatise on the Mathematical Theory of Elasticity, 4th ed. Cambridge University Press, Cambridge, pp. 381–398 Chapter 18.

Mielke, A., Holmes, P., 1988. Spatially complex equilibria of buckled rods. Arch. Rat. Mech. Anal. 101, 319–348.

Press, W.H., Flannery, B.P., Teukolsky, S.A., Vetterling, W.T., 1986. Numerical Recipes: the Art of Scientific Computing. Cambridge University Press, Cambridge.

Thompson, J.M.T., Champneys, A.R., 1996. From helix to localised writhing in the torsional post-buckling of elastic rods. Proc. Roy. Soc. Lond. A 452, 117–138.